FREQUENCY SELECTIVE SURFACES: DESIGN OF BROADBAND ELEMENTS AND NEW FREQUENCY STABILIZATION TECHNIQUES

Adriano P. Raiva*, Frances J. Harackiewicz*, and Jefferson Lindsey III**
*Department of Electrical and Computer Engineering
**Department of Technology
Southern Illinois University Carbondale
Carbondale, Illinois 62901

Abstract: Two important features of a frequency selective surface (FSS) are bandwidth and frequency stability. Methods of increasing FSS bandwidth include, among others, decreasing inter-element spacing and increasing the thickness of the supporting dielectric layer. The shape of the FSS element also determines its bandwidth. To achieve any desired bandwidth, a combination of these methods is often required. The present work focuses on designing an FSS element where shape alone is the most important feature in determining its bandwidth. The elements are a combination of two known FSS elements with close resonant frequencies but not located in the same frequency band. The FSS's are designed to act as reflectors. The second part of this paper discusses frequency stabilization techniques, focusing on rectangular arrays of tripoles and cross dipoles. These elements have poor frequency stability with angle of incidence for parallel polarization. Dielectric loading and skewed arrays help minimize the problem. In the present work, a new method based on varying the element's impedance by partially removing the conducting patch at the center of the element is introduced.

1. Introduction

Broadband frequency selective surfaces often require the design of closely packed arrays of FSS elements or the increase of thickness of the supporting dielectric material [1, 2]. New techniques such as genetic algorithm [3] can deliver an FSS with a desired bandwidth at the expense of higher computation time. In the present work, an FSS element with broadband characteristics designed as a combination of known elements is presented. At first, multiband frequency selective surfaces are discussed. Double-Ring (DR) and Double Square Loop (DSL) FSS [1] have proven to be good single layer, dual band FSS. More recently the use of fractal geometries [4-7] in FSS applications has made possible the design of single layer dual or tri-band FSS, which is a great advantage since multiband FSS were designed using multiple layer frequency selective surfaces. However, resonant frequencies of fractal, double ring, or double square loop frequency selective surfaces are not closely located. This is because most designs require that these frequencies be located at different frequency bands and the design of fractal, DR or DSL FSS with close resonant frequencies is not possible. However, these FSS's are important when making a comparative study of resonant frequency placement in a dual band FSS.

The design of broadband elements begins with a comparative study of dual-band FSS's made of elements of different shapes. Later the elements are chosen according to features such as how close their resonant frequencies can be, their resonant frequency stability, and their bandwidth. At the end, a new FSS element is created.

The second part of this paper analyzes the frequency stabilization of rectangular arrays of tripole and cross dipole FSS with the angle of incidence. The goal is to show that even without skewed arrays it is possible to avoid frequency drift with the angle of incidence provided that part of the patch at the center of elements is removed. Skewed and closely packed arrays create very large bandwidths which may not be desirable if the FSS is to be used as subreflector at frequencies that are not too far apart. Numerical and experimental results will be discussed in both cases.

2. From Multiband to Broadband FSS. A Comparative Study of Resonant Frequency Location.

We begin our analysis with the study of fractal FSS. For our purpose, only one type of fractal structure will be discussed, and it is shown in Figure 1. Figure 1 shows a fractal structure of inset cross dipoles. It is important to emphasize that this fractal structure is a combination of two arrays: one formed by the larger cross dipoles of the 0^{th} iteration, and the second array formed by the smaller cross dipoles of the 1^{st} iteration. Each array can be analyzed separately as an FSS, which allows us to change the properties of elements of one iteration leaving the elements of the other iteration unchanged. Fractal geometries such as Sierpinski carpet, Sierpinski gasket or Koch patch would not serve our purposes since the different stages cannot be analyzed and manipulated separately.

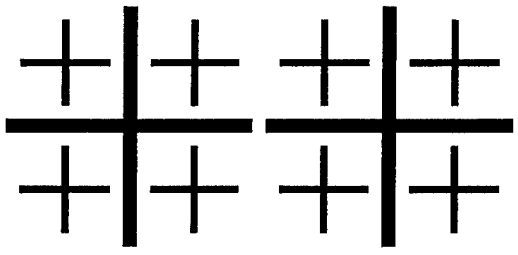

Figure 1. Inset cross dipole fractal FSS.

Fractal structures such as the shown in Figure 1 have been extensively analyzed [4] and their features as dual band FSS have been verified. Therefore they will not be analyzed in this paper. Due to space limitation, the size of cross dipole of the 1st iteration on Figure 1 can not be increased such that its resonant frequency is close to that of the cross dipole of the 0th iteration. The lowest resonant frequency of the 1st iteration can be at least twice of the resonant frequency of the 0th iteration. It is therefore necessary to change the elements of the 1st iteration if we want to bring its resonant frequency close to that of the first stage cross dipole. The changes of elements in the 1st iteration will be made such that their resonant frequency decreases gradually in order to analyze carefully their influence on transmission properties of the FSS. At this stage of our analysis, the shape of the element is irrelevant and only the location of the second resonant frequency is of the utmost importance.

We start by replacing the smaller cross dipoles of the 1st iteration in Figure 1 by tripoles, and the resulting non-fractal structure is shown in Figure 2.

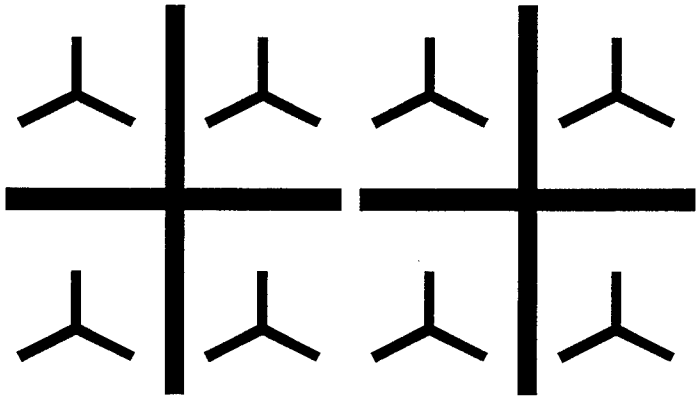

Figure 2. Modified structure from Figure 1 with the smaller cross dipoles replaced by tripoles.

The FSS shown in Figure 2 was analyzed for the dimensions shown in Table 1. The computed results in Figure 3 are for normal incidence and parallel polarization. The two resonant frequencies are not close, but at least the resonant frequency of the tripole is less than twice the frequency of cross dipole. This could not be achieved with fractal structures since we do not want to increase the FSS's cell size.

Table 1. Parameters of the arrays in Figure 2.

Element	length L, mm	Width w, mm	periodicity in x direction Tx, mm	periodicity in y direction Ty, mm
cross dipole	11	0.5	16.4	16.4
tripole	3.5	0.3	8.2	7.4

The array of Figure 2 is printed on a dielectric material with $\varepsilon_r = 4.5$ and thickness t = 30 mil (0.762 mm). The transmission characteristics are shown in Figure 3, and the transmission coefficients of each array as a separate FSS are also shown. The transmission characteristics of the tripole FSS alone, cross dipole FSS alone, and the combination of both elements as in Figure 3 are similar to the transmission characteristics of fractal structures shown in [4].

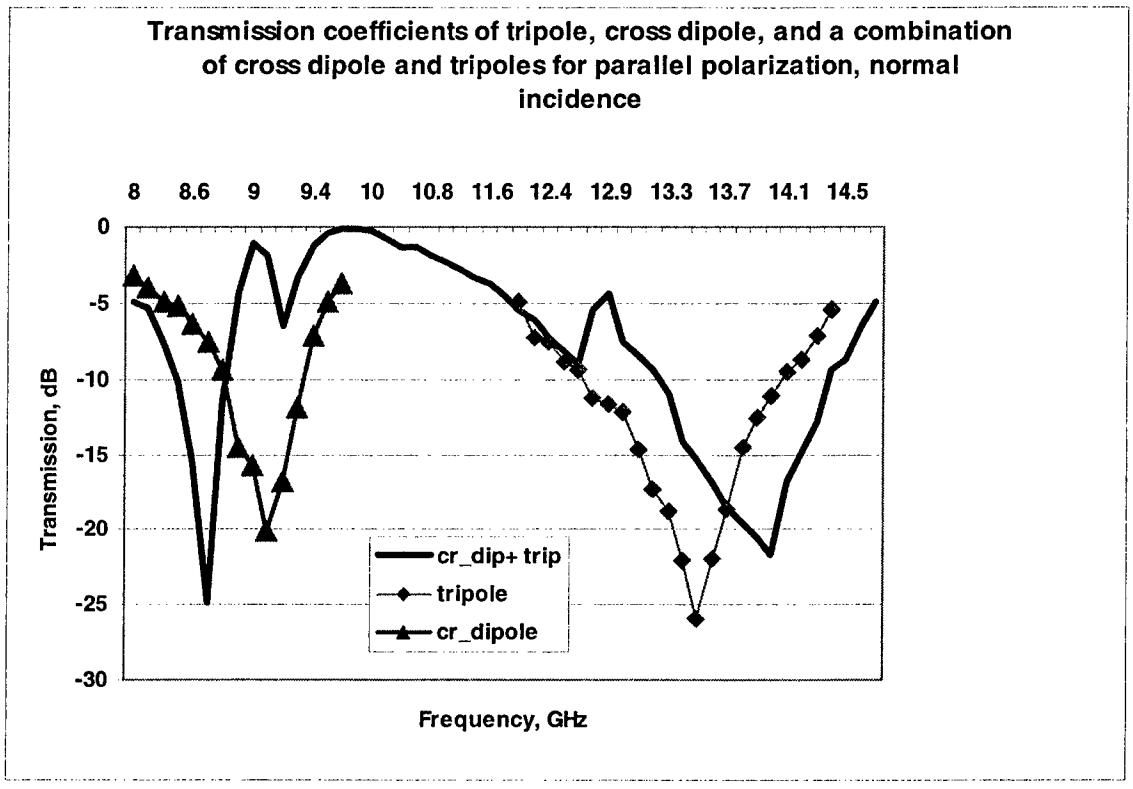

Figure 3. Computed transmission coefficients of tripole, cross dipole, and the combination of both as shown in Figure 2.

The graph shows that combining tripoles and cross dipoles in the same unit cell gives similar transmission characteristics to those of FSS made of each element separately. The graphs are for normal incidence, parallel polarization. Ansoft HFSS was used to compute the transmission coefficients.

If we want the two resonant frequencies to be even closer to each other, we need to change the tripole with an element of much lower resonant frequency. In Figure 4 the tripoles of Figure 2 have been replaced by Jerusalem crosses and the transmission characteristics have been computed similarly to Figure 3.

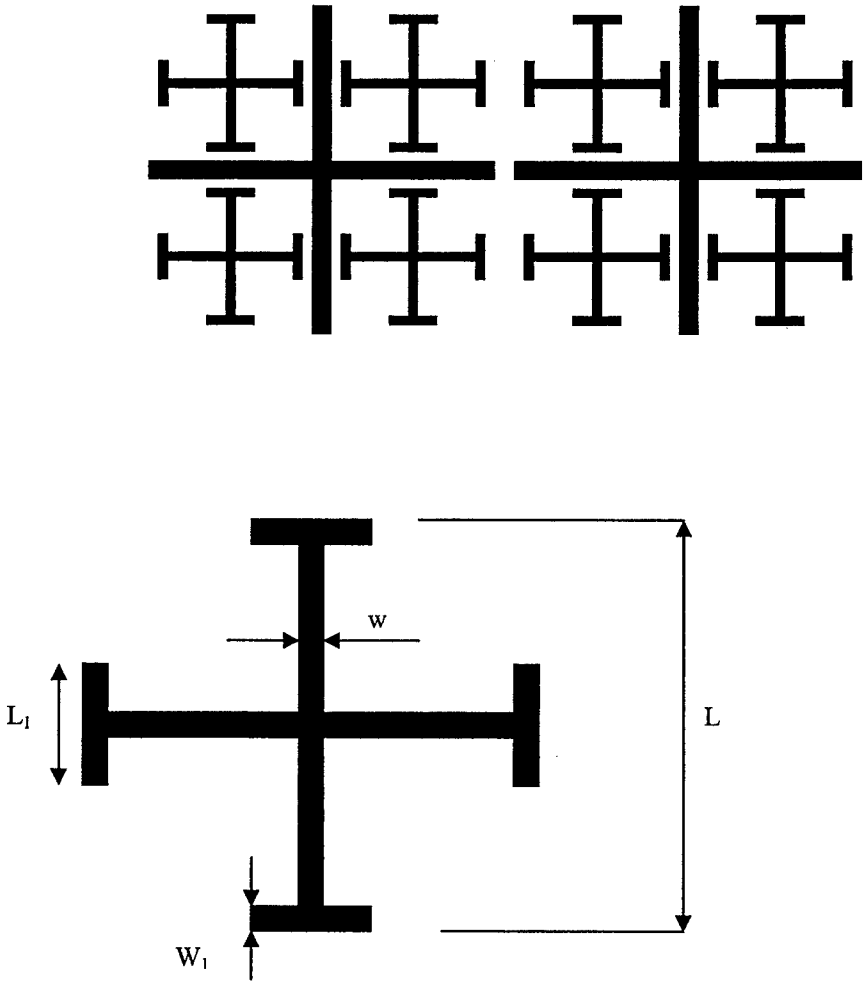

Figure 4. *Top.* Modified structure from Figure 2 with the second stage tripoles replaced by Jerusalem crosses. *Bottom:* Jerusalem cross.

Figure 5 shows the transmission coefficients of cross dipole, Jerusalem cross and the combination of both as shown in Figure 4. The parameters of the array of Figure 4 are given in Table 2, and like in Figure 2, the computation was made for a supporting dielectric layer of $\varepsilon_r = 4.5$ and thickness of 30 mil (0.762 mm). It is important to notice that the resonant frequency of the tripole is 13.5 GHz and that of Jerusalem cross is 12.5 GHz as shown in figures 3 and 5, respectively. The Jerusalem cross did manage to drop the second resonant frequency. The first resonant frequency for the combined elements in Figure 2 is 8.7 GHz while the same frequency for the arrangement in Figure 4 is 7.5 GHz as it is shown in figures 3 and 5, respectively. The difference between the second and the first resonant frequencies drops from 5.2 GHz in Figure 3 to 4.7 GHz in Figure 5 for the combined elements.

Table 2. Parameters of the arrays in Figure 4.

Element	length L, mm	Width w, mm	periodicity in x direction Tx, mm	periodicity in y direction Ty, mm
cross dipole	11	0.5	16.4	16.4
Jerusalem cross*	6.4	0.6	8.2	8.2

**Jerusalem cross end loading bars dimensions are* $w_l = 0.2$ mm $L_l = 2.0$ mm

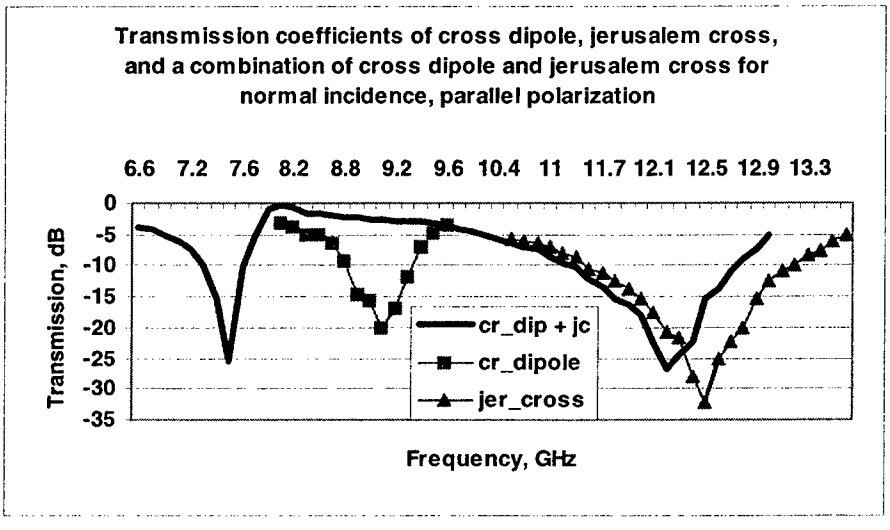

Figure 5. Computed transmission coefficients of cross dipole, Jerusalem cross and the combination of both. The first and second resonant frequencies of the arrangement in Figure 4 get slightly closer, but the results are still far from the desired.

From the arrangement in Figure 4 and the corresponding graph in Figure 5 it is clear that the first and the second resonant frequencies are as close as possible for this geometry. To overcome the problem, another change on element shape is needed. We replace the cross dipole with a ring, and the arrangement is shown in Figure 6. Also the dielectric material was changed to $\varepsilon_r = 10.2$ and thickness = 25 mil (0.64 mm). The change of dielectric constant was made in order to reduce the size of the ring needed to obtain a resonant frequency similar to that of the replaced cross dipole. The inner and the outer radiuses of the ring are 3 mm and 3.5 mm respectively. The length and width of the Jerusalem cross are L = 5.4 mm and w = 0.5 mm, and the Jerusalem cross end loading bars dimensions are $w_l = 0.2$ mm, and $L_l = 1.9$ mm.

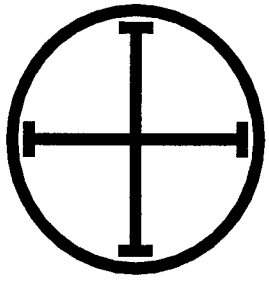

Figure 6. Ring and Jerusalem cross are the elements that have the closest resonant frequencies.

Figure 7 shows the transmission coefficients of ring, Jerusalem cross, and the combination of both. Analyzing the graphs of Figure 7, we can notice that as the resonant frequencies of the elements get closer, the resonant frequencies of the combined elements do not get closer. They actually are farther apart compared to the arrangements of Figures 2 and 4. The difference between the second and the first resonant frequencies of the combined ring and Jerusalem cross arrangement is 6.6 GHz, which is more that the differences of the previous arrangements of Figures 2 and 4. This is because since the two resonant frequencies are not in the same reflection band the Foster's reactance theorem [2] must apply. This theorem states that between two nulls there must be a pole and vice versa. That explains why the resonant frequencies of the ring and Jerusalem cross are much different to their values in a combination ring-Jerusalem cross. If the resonant frequencies of ring and Jerusalem cross were located in the same frequency band we could immediately have a broadband FSS [8], but due to the size restrictions, we cannot make the frequencies any closer. However, we can notice that the second reflection band is becoming much larger than in the previous cases, and we need to use this characteristic to make our broadband FSS. One way to accomplish our objective is to connect the ring and the Jerusalem cross, forming one single element as shown in Figure 8. The transmission coefficient of the element of Figure 8 is shown in Figure 9,

and it is compared with the second reflection band of the combination ring-Jerusalem cross. As it can be seen from the graphs in Figure 9, our new element has a much larger bandwidth compared to the unconnected ring-Jerusalem cross pair. Note: The ring plus the Jerusalem cross FSS is found to be transparent at 6.5 GHz while acting as a reflector at 5.7 and 12.5 GHz. Figure 10 shows the numerical and measured transmission characteristics of the new element, and Figure 11 shows the FSS board used for measurement results on Figure 10.

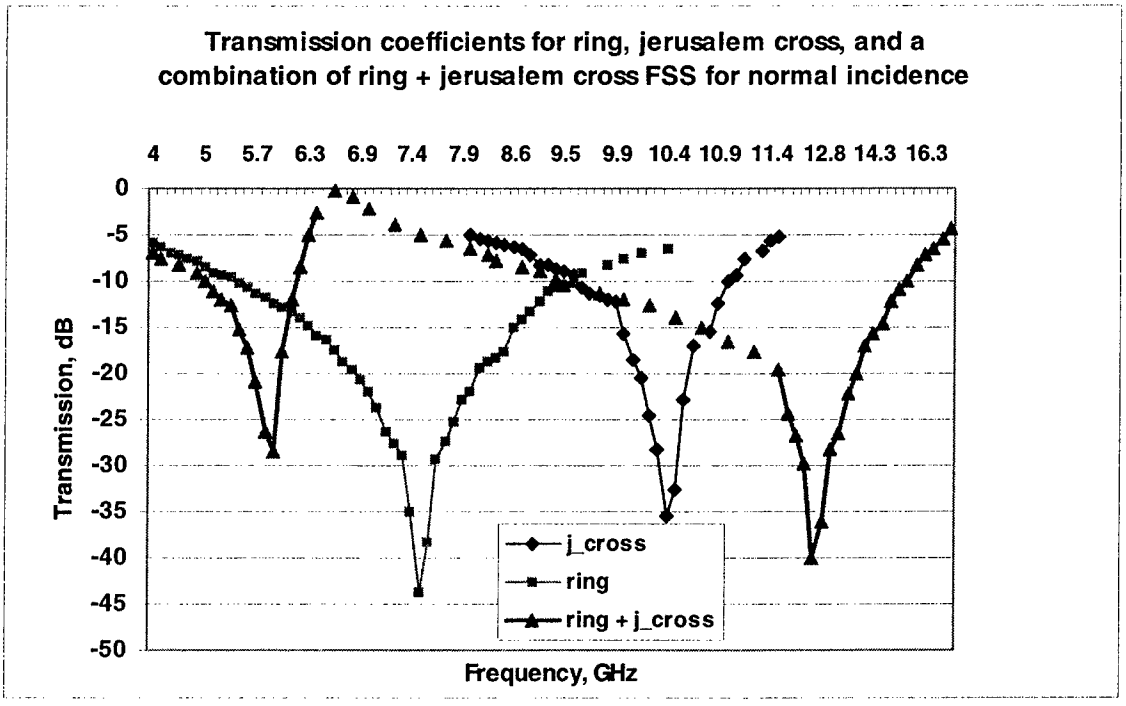

Figure 7. Computed transmission coefficients of ring, Jerusalem cross, and a combination ring-Jerusalem cross. The periodicity of the elements is 7.5 mm in both x and y directions.

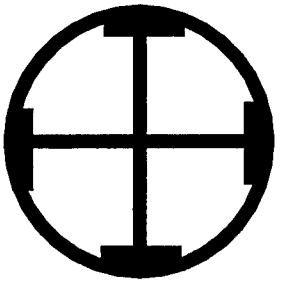

Figure 8. Ring and Jerusalem connected to form one single element in order to get broadband characteristics.

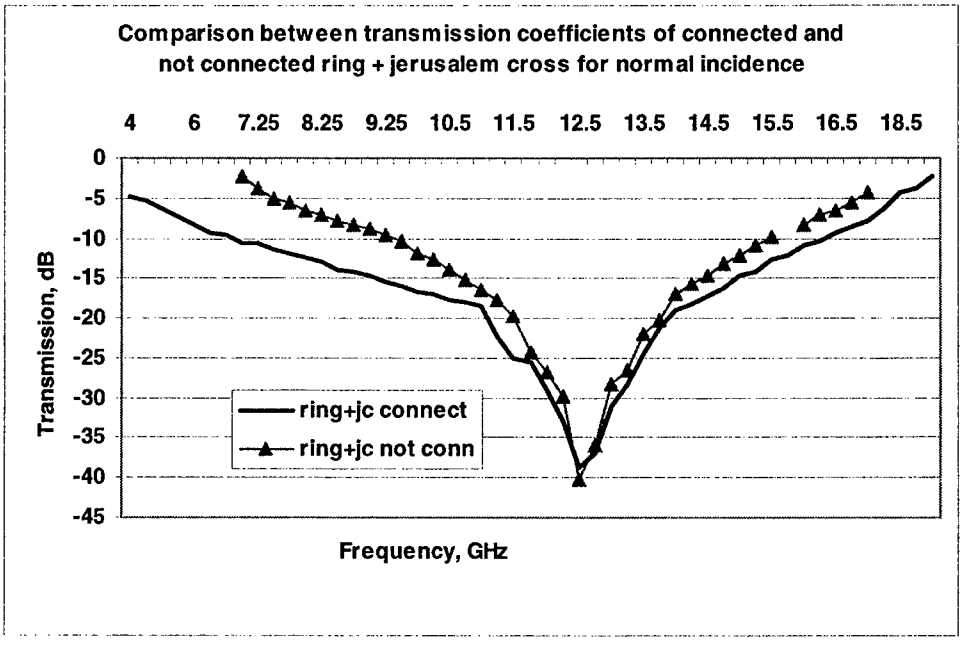

Figure 9. Comparison of computed transmission coefficients of unconnected ring + Jerusalem cross (second reflection band) and the same elements connected. From the graphs, it is clear that connecting both elements increases the bandwidth of the reflection band.

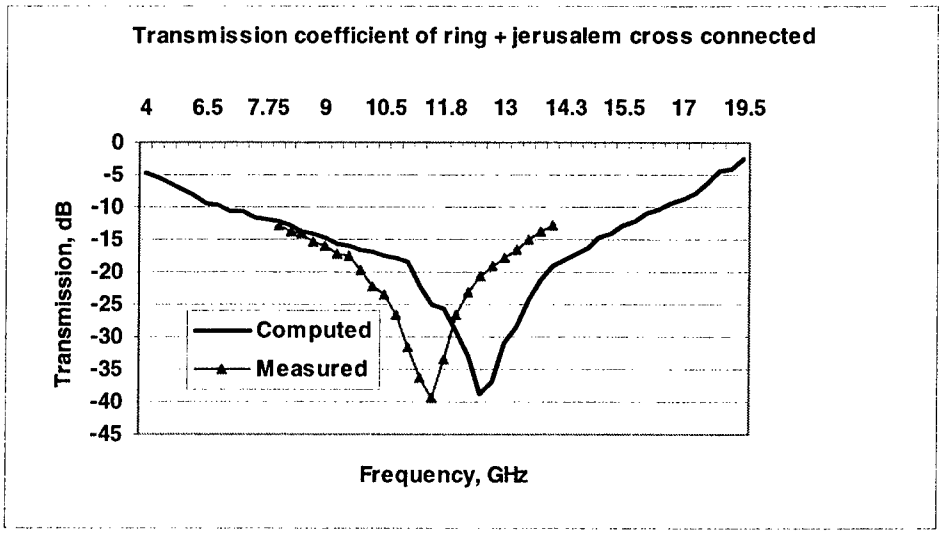

Figure 10. Computed and measured transmission coefficients of the new element shown in Figure 8. .

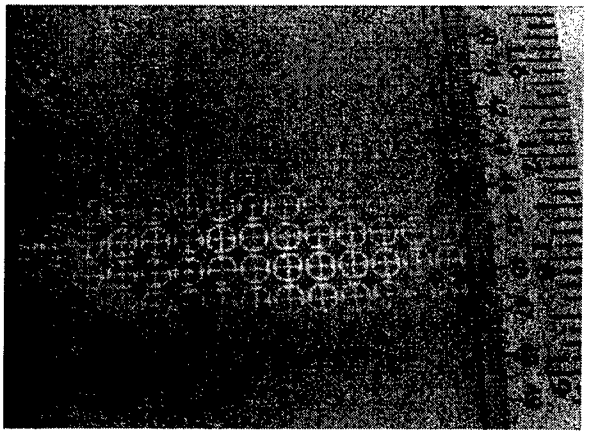

Figure 11. FSS used for measurement results shown in Figure 10. The dielectric material is RT/Duroid with ε_r = 10.2, and thickness = 25 mil (0.64 mm). The size of the FSS is 18 inches x 18 inches.

Table 3 shows a comparison of the bandwidths between the Jerusalem cross, ring, combination ring-Jerusalem cross, and the new element.

Table 3. Comparison of the frequency characteristics of elements used in the making of the new FSS element.

	Center Frequency (GHz)	Bandwidth (GHz)	Bandwidth (%)
Jerusalem Cross	10.4	1.5	14.42
Ring	7.5	4	53.3
Ring + Jerusalem Cross Disconnected	11.5	6	52.17
Ring + Jerusalem Cross Connected	11.5	9.5	82.6

As seen in Table 3 the new element has a bandwidth of 9.5 GHz which is 2.375 times the bandwidth of the ring element, 6.3 times the bandwidth of Jerusalem cross, and 1.58 times the bandwidth of the combination ring-Jerusalem cross. These properties are remarkable, since most of the common elements would require a sandwich FSS to achieve such a large bandwidth.

2.1. Broadband Element Based on Combination of Square Loop and Jerusalem Cross

Based on the analysis previously formulated, another element with broadband characteristics similar to the element of connected ring-Jerusalem cross was obtained. This element is the combination of square loop and Jerusalem cross. Figure 12 shows the broadband element, and Figure 13 shows its transmission coefficient for normal incidence.

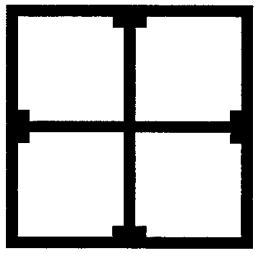

Figure 12. Square loop and Jerusalem cross connected in order to from a broadband element. The approach is similar to the presented in figure 8. The dimensions used for computation coefficients are: the outer and inner dimensions of the loop are 6mm and 5.4 mm, respectively. The length of the Jerusalem cross is 5.2 mm, width w = 0.5 mm, and the end loading bars dimensions are L_l = 1.9 mm, w_l = 0.2 mm.

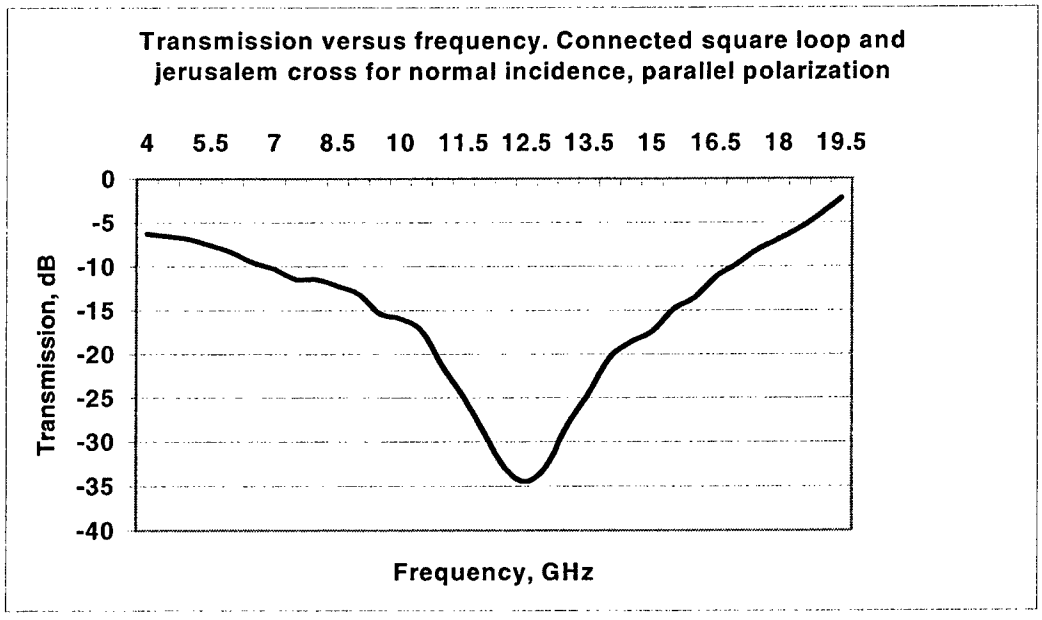

Figure 13. Computed transmission coefficient of the element shown in figure 12 for normal incidence. The dielectric material is RT/Duroid with thickness 0.64 mm and ε_r = 10.2.

3. Frequency Stabilization Technique for FSS made of Rectangular Arrays of Tripoles and Cross Dipoles

Tripoles and cross dipoles have the following principal characteristics:

a) The fundamental mode is strongly excited when the element length is about $\lambda/2$, and the incident E-field has a component parallel to the elements.
b) An odd mode is excited only for oblique angles of incidence, and when the element length is approximately λ.
c) The inter-element spacing plays a big role. Decreasing the inter-element spacing increases the bandwidth and delays the onset of grating lobes. This feature is common for every type of FSS elements.

For the tripole FSS in particular, a skewed array is highly recommended since it not only increases frequency stability with angle of incidence but also solves the problem of cross polarization making the cross polarization frequency identical to the parallel polarization.

The analysis on frequency stabilization will be centered on tripole and cross dipole rectangular arrays of FSS. Studies on skewed arrays did not bring good results especially for cross polarization on tripole arrays where the cross polarization transmission coefficient was not lower than –10 dB over the entire reflection band. One of the

objectives was to keep the dual polarization characteristics of the elements. The design parameters were chosen as follows:

i) The inter-element spacing was made as large as possible without generating grating lobes. That would reduce the bandwidth and allow a better analysis of resonant frequency drift with angle of incidence for parallel incident E-fields.

ii) The remaining parameters such as resonant frequency, length and width of the elements, dielectric constant and thickness of the supporting dielectric materials, were chosen such that experiments could be performed with the existing measurement facilities at Southern Illinois University.

The frequency stabilization method presented is based on the theory of variable surface impedance [9] used to change the transmission and reflection properties of an FSS. Once the shape, array element and the unit cell dimensions are fixed, an additional method of changing the frequency response is through the application of a varying surface impedance as shown in Figure 14. The addition of element losses began with the application of a constant resistive boundary condition on the tangential electric fields at the surface of the conductor, and this was later applied to periodic surfaces. The resistive boundary condition evolved from the application of the boundary condition to thin metallic surfaces. The general equation is

$$\vec{E}^{inc} + \vec{E}^{scat} = Z_s \vec{J}_s \tag{1}$$

where the surface impedance is given by Z_s. The two limiting cases of this equation occur when $Z_s = 0$ and Z_s approaches infinity. When $Z_s = 0$ the boundary condition enforced by equation (1) is a PEC boundary, and when $Z_s \rightarrow \infty$ the surface currents are forced to zero, and the surface no longer scatters energy. In the current analysis the case of $Z_s \rightarrow \infty$ is applied given that for both tripole and cross dipole the surface impedance of the element is changed by removing the conducting material at its center as shown in Figure 15.

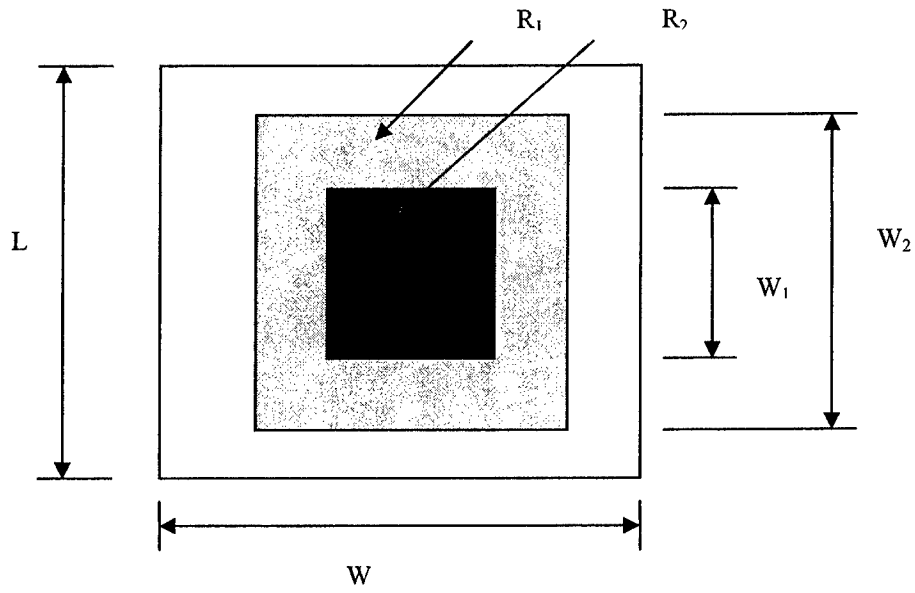

Figure 14. Example of a unit cell geometry showing varying surface impedances R_1 and R_2.

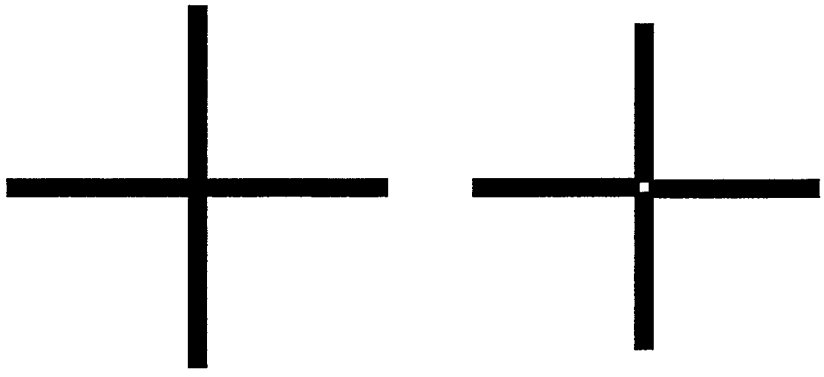

a)

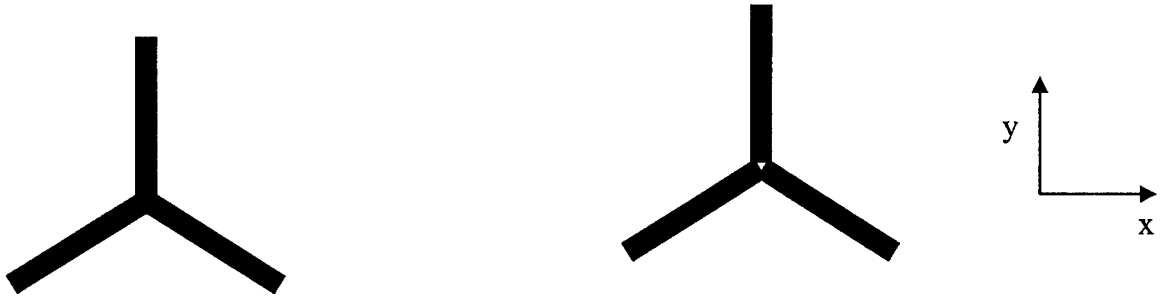

b)

Figure 15. a) Cross dipole and b) tripole with and without removed conducting patch at the center. Removing the conducting material at the center of element implies a variation of impedance from $Z_s = 0$ to $Z_s \rightarrow \infty$.

3.1. Analysis of Tripole Array

Theoretical and measured results were obtained for tripole arrays [2, 10] and for tripole arrays with removed conducting material at its center. The length and width of the tripoles were 4 mm and 0.6 mm respectively, and the area of the removed conducting material is a triangle with side length 0.6 mm. The performances of the arrays have been examined for two principal orientations relative to the incident plane wave. In the first orientation, the tangential component of the electric field is parallel to the top arm of the tripole (y-axis), and in the second orientation, they are perpendicular to each other. The resonant frequency is within the X-band frequency. The tripole array was printed on a dielectric substrate with thickness of 20 mil (0.508 mm), ε_r = 4.5, and inter-element spacing of 12 mm. A second dielectric with the same parameters was placed on top of the arrays forming a sandwich FSS. Figure 16 shows the transmission response of a tripole array. Ansoft HFSS was used for computation of the transmission responses.

The graphs on Figure 16 show that for parallel polarization the resonant frequency drifts when the angle of incidence varies from 0^0 to 45^0. Figure 17 shows comparison of transmission coefficients of tripole FSS rectangular arrays with and without removed conducting patch. Other studies conducted by the authors show that the resonant frequency drifts downwards when part of the conducting material is removed. The amount of drift depends on the area and shape of the conducting material removed. Removing large areas of conducting material can result in greater resonant frequency drift.

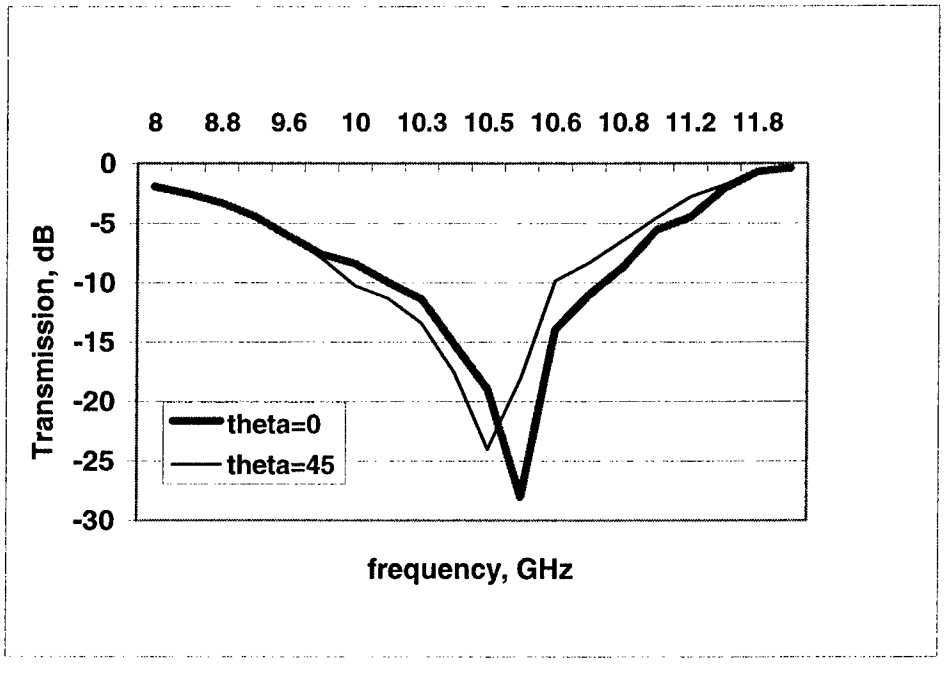

Figure 16. Computed transmission coefficient of rectangular arrays of tripole FSS, parallel polarization for angles of incidence of 0^0 and 45^0.

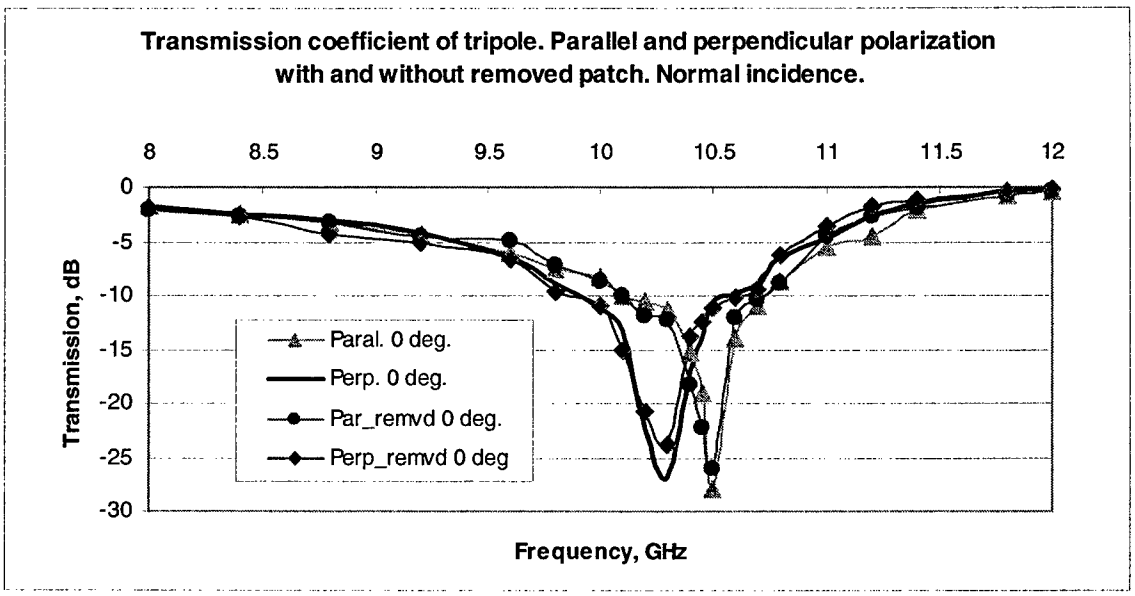

Figure 17. Comparison of computed transmission coefficients of tripole and tripole with removed conducting material for normal incidence, parallel and perpendicular polarization. The graphs are very similar since the area removed is small

Figure 18 shows transmission coefficient for parallel polarization for angles of incidence of 0^0 and 45^0. As it is shown in Figure 18 and in contrast with the tripole shown in Figure 16, there is no frequency drift when the angle of incidence is shifted from 0^0 to 45^0. Transmission coefficient for perpendicular polarization differs from that of parallel polarization for rectangular arrays as shown in Figure 19. To compensate the difference the length of the upper arm of the tripole was increased in order to lower the resonant frequency of the parallel polarization and make it equal to that of perpendicular polarization as shown in Figure 20. This is because increasing the length of the tripole's upper arm only influences parallel polarization keeping the perpendicular polarization unchanged. Figure 21 shows the FSS used for measurements, and it uses modified tripoles shown in Figure 20.

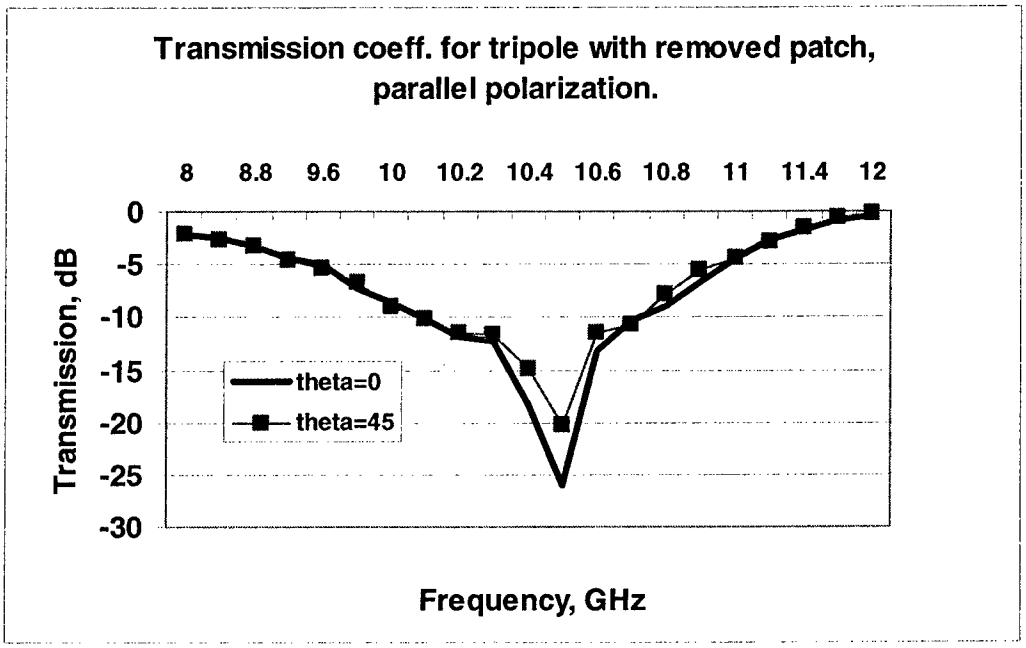

Figure 18. Computed transmission coefficients of tripole with removed conducting patch, parallel polarization, incidence angles of 0^0 and 45^0. The figure shows that there is no frequency drift with the change of incidence angle as in Figure 16.

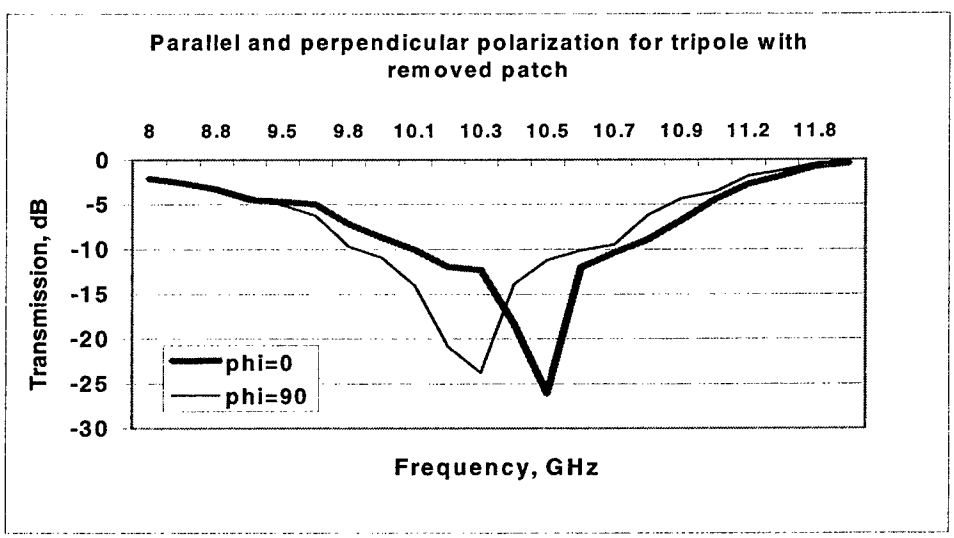

Figure 19. Transmission coefficients for parallel (phi=0) and perpendicular (phi=90) polarizations, normal incidence of tripole with removed patch.

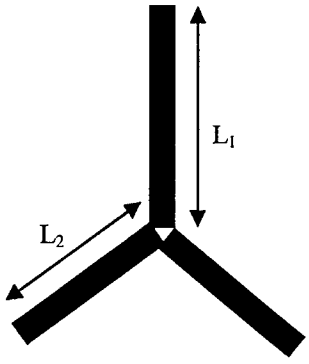

Figure 20. Modified tripole with removed patch. Increasing properly the length of the upper arm of the tripole drops the resonant frequency of parallel polarization to a value equal to that of the perpendicular polarization.

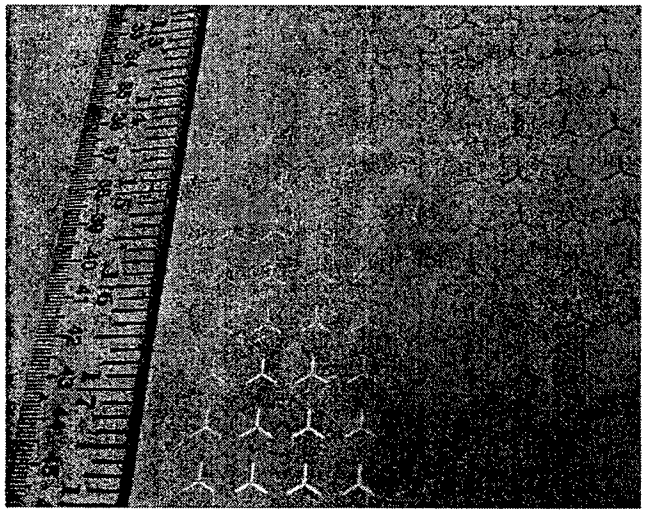

Figure 21. Printed tripoles with removed patch on a dielectric substrate used for measurements. The shown FSS was covered by a dielectric with similar properties. The array covers an area of 18"x18". The inter-element spacing is 12mm, the tripole length is: upper arm $L_1 = 4.1$ mm, other arms $L = 4$ mm, width = 0.6 mm. Dielectric thickness = 20 mil (0.508 mm), $\varepsilon_r = 4.5$.

Figure 22 a) shows the computed transmission coefficient of the modified tripole with removed patch for both parallel and perpendicular polarization. As it is shown there is no more difference between the parallel and perpendicular polarization frequencies. The length of the upper arm of the tripole has been increased by 0.1 mm. Figure 22 b) shows the measured results for the same case. As it is shown, there is little difference between computed and measured results.

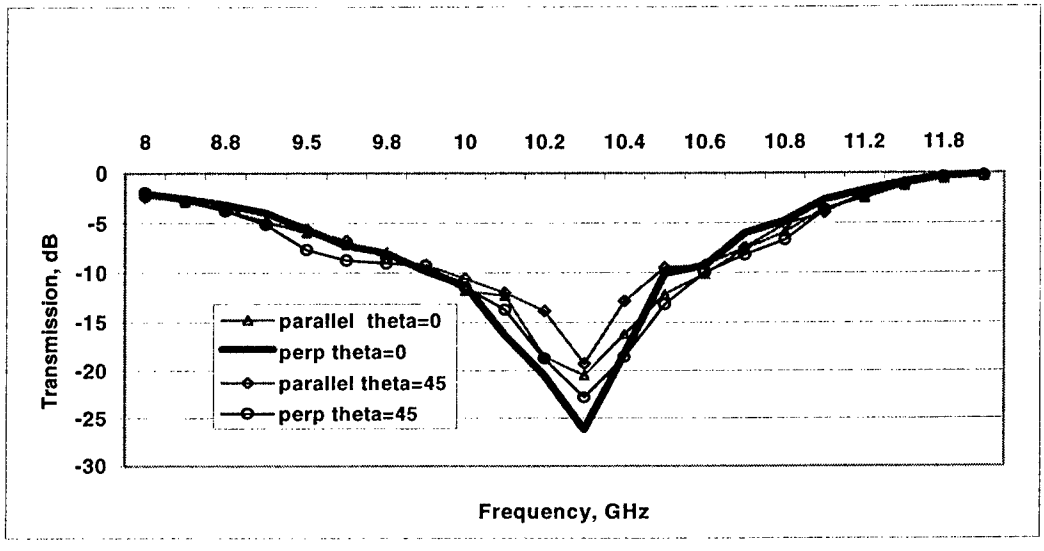

a)

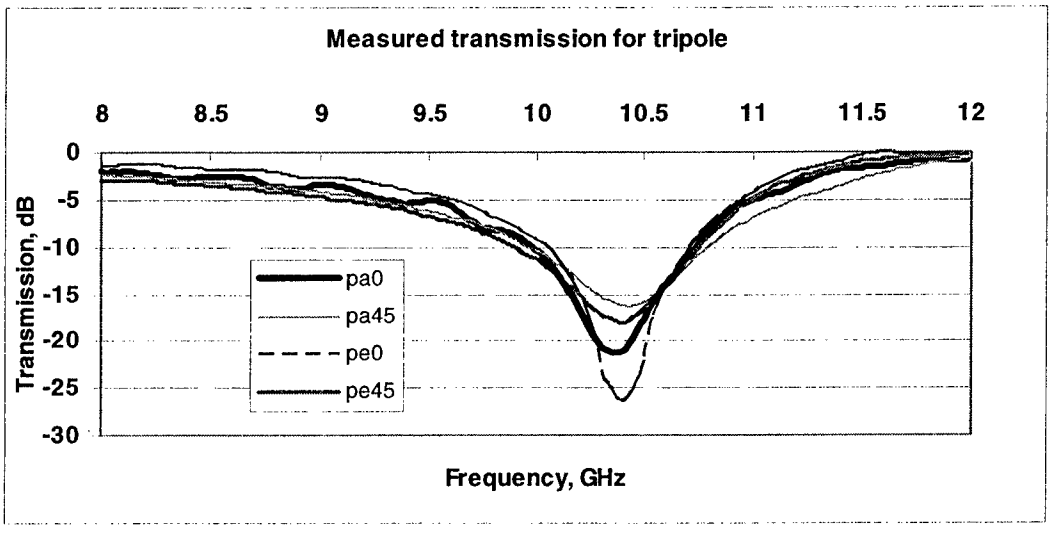

b)

Figure 22. a) Computed and b) measured results for modified tripole with removed patch.

3.2. Analysis of Cross Dipole Array

Similar analysis was made for cross dipole array. The cross dipole length and width were 6 mm and 0.6 mm respectively, and the inter-element spacing was 10 mm. As with the tripole arrays, the array of cross dipoles was printed on a dielectric material with thickness of 20 mil (0.508 mm) and $\varepsilon_r = 4.5$. Another dielectric with the same properties was placed on top forming a sandwiched FSS. Figure 23 shows computed transmission coefficients of cross dipole for angles of incidence of 0^0 and 45^0. As shown in this figure, there is a frequency drift when the angle of incidence is changed from 0^0 to 45^0. Figure 24 shows the transmission coefficients of cross dipole and cross dipole with removed patch, and the area removed is a square with sides of 0.2 mm. In this figure, it is clear that the resonant frequency drops when part of the conducting patch is removed. Figure 25 shows the transmission coefficients of cross dipole with removed patch for incident angles of 0^0 and 45^0. Similarly to the tripole case there is no frequency drift when part of conducting patch at the center of cross dipoles is removed.

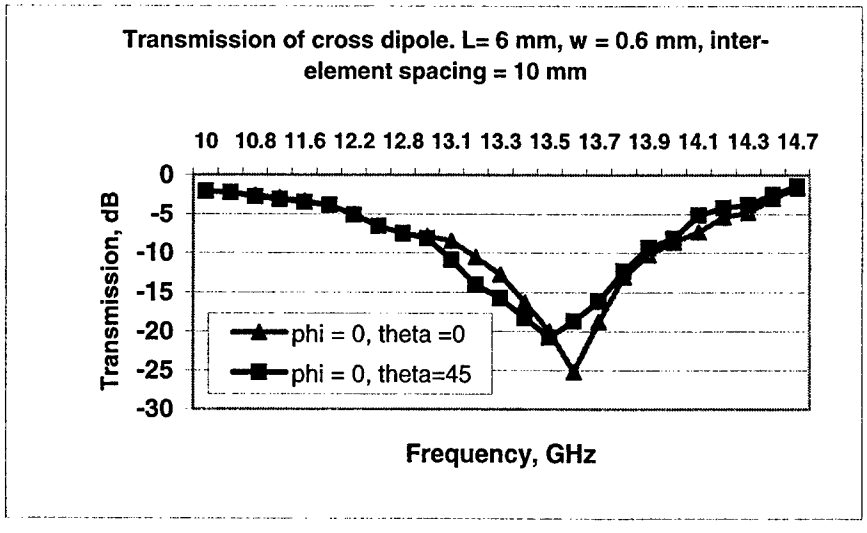

Figure 23. Computed transmission coefficients of cross dipole FSS for incidence angles of 0^0 and 45^0.

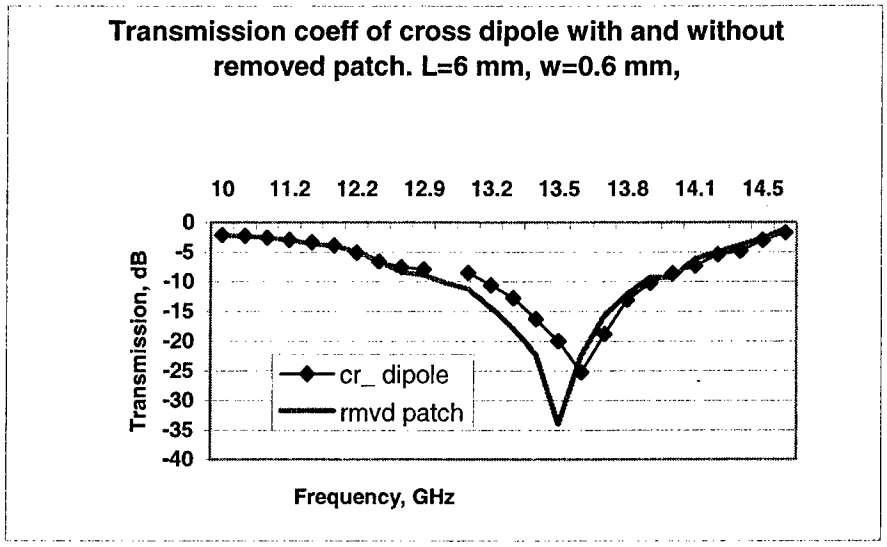

Figure 24. Computed transmission coefficients of cross dipoles with and without removed conducting patch for normal incidence.

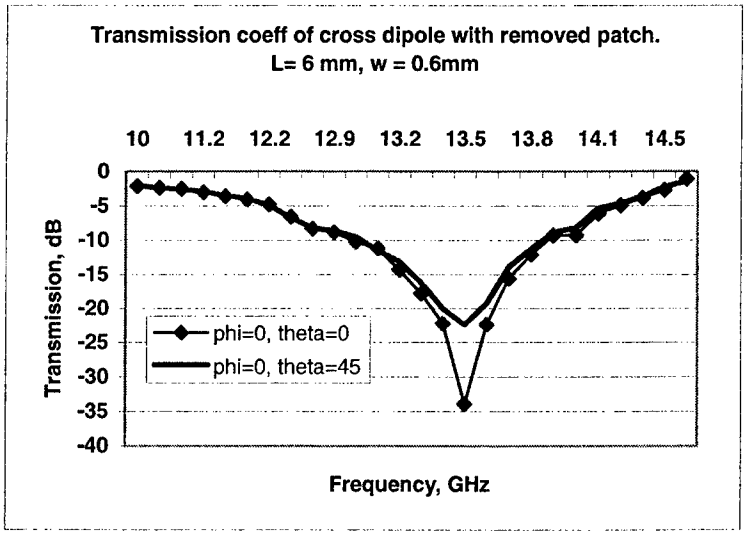

Figure 25. Computed transmission coefficients of cross dipole with removed conducting patch for angles of incidence 0^0 and 45^0.

4. CONCLUSIONS

In this paper two different topics were discussed: design of single layer broadband FSS element, and a frequency stabilization technique for tripole and cross dipole rectangular arrays of FSS. The broadband FSS design was based on analysis of transmission characteristics of double band, single layer FSS. Special attention was focused on the study of how the transmission characteristics of the double band FSS behave when the resonant frequencies of the two reflection bands are placed close to each other. It was found that as the two resonant frequencies get closer, the second reflection band gets wider. Due to the Foster's reactance theorem, the lower resonant frequency drifts to a lower value in order to get a pole between the two nulls. This particular feature was used to create a broadband FSS by connecting together two elements to form a single element with desirable broadband characteristics. Two broadband elements were formed by first connecting a Jerusalem cross with a ring, and later connecting a Jerusalem cross with a square loop. Their transmission characteristics were presented, and some measured results were shown.

With regards to the frequency stabilization technique it was found that removing part of the conducting patch at the center of tripoles and cross dipoles could prevent frequency drift with the angle of incidence. By removing part of the conducting patch of the element, the surface impedance of the element varies and this produces the change in the transmission characteristics. For tripole elements the upper arm must be increased to match the resonant frequencies of parallel and perpendicular polarizations.

REFERENCES

[1] T. K. Wu, *Frequency selective surfaces and grid Array*, John Wiley & Sons INC, 1995.

[2] Ben A. Munk, *Frequency Selective Surfaces. Theory and Design*, John Wiley & Sons, INC, 2000

[3] Sourav Chakravarty, Raj Mittra, "Application of Microgenetic Algorithm (MGA) to the Design of Broad-band Microwave Absorbers using Multiple Frequency Selective Surface screens buried in Dielectrics", *IEEE Transactions on Antennas and Propagation,* vol. 30 no. 3 pp 284-296, March 2002

[4] John P. Gianvittorio, Yahya Rahmat-Samii, and Jordi Romeu, "Various self-Similar Geometries Used for Dual-Band and Dual-Polarized FSS", *www.ee.ucla.edu/~johng/research.html,* accessed 11/10/2002

[5] Jordi Romeu and Yahia Rahmat-Samii, "Fractal Based FSS with Dual Band Characteristics, *IEEE Antennas and Propagation Society International Symposium*, Vol. 3 pp 1734-1737, 1999

[6] Jordi Romeu and Yahia Rahmat-Samii, "Fractal FSS: A Novel Dual-Band Frequency Selective Surface", *IEEE Transactions on Antennas and Propagation,* Vol. 48 No. 7 pp1097-1105, July 2000.

[7] Douglas H. Werner, Suman Ganguly, "An Overview of Fractal Antenna Engineering Research", *IEEE Antennas and Propagation Magazine,* Vol. 45 No. 1, pp 38-57, February 2003

[8] D. Sarkar, P. P. Sarkar, S. Das, and K.Chowdhury, "An Array of Stagger-Tuned Printed Dipoles as a Broadband Frequency Selective Surface" *Microwave and Optical Technology letters,* Vol. 35 No. 2, October, 2002

[9] Larry W. Epp, *Frequency Selective Surfaces with Lumped and Time Varying Loads, Variable Surface Impedance, and Multiple Screens,* Ph.D Dissertation, University of Illinois at Urbana-Champaign, 1990

[10] P. W. B. Au, L. S. Musa, E. A. Parker, R. J. Langley, "Parametric Study of Tripole and Tripole loop arrays as Frequency Selective Surfaces", *IEE Proceedings,* Vol. 137, Pt. H, No. 5 pp. 263-268, October 1990.